Accretion and destruction of planetesimals in turbulent disks

Shigeru Ida

Tokyo Institute of Technology, Ookayama, Meguro-ku, Tokyo 152-8551, Japan

ida@geo.titech.ac.jp

and

Tristan Guillot, Alessandro Morbidelli

Observatoire de la Côte d'Azur, CNRS UMR 6202, BP 4229, 06304 Nice Cedex 4, France

guillot@oca.eu, morby@oca.eu

ABSTRACT

We study the conditions for collisions between planetesimals to be accretional or disruptive in turbulent disks, through analytical arguments based on fluid dynamical simulations and orbital integrations. In turbulent disks, the velocity dispersion of planetesimals is pumped up by random gravitational perturbations from density fluctuations of the disk gas. When the velocity dispersion is larger than the planetesimals' surface escape velocity, collisions between planetesimals do not result in accretion, and may even lead to their destruction. In disks with a surface density equal to that of the "minimum mass solar nebula" and with nominal MRI turbulence, we find that accretion proceeds only for planetesimals with sizes above $\sim 300\,\mathrm{km}$ at 1AU and $\sim 1000\,\mathrm{km}$ at 5AU. We find that accretion is facilitated in disks with smaller masses. However, at 5AU and for nominal turbulence strength, km-sized planetesimals are in a highly erosive regime even for a disk mass as small as a fraction of the mass of Jupiter. The existence of giant planets implies that either turbulence was weaker than calculated by standard MRI models or some mechanism was capable of producing Ceres-mass planetesimals in very short timescales. In any case, our results show that in the presence of turbulence planetesimal accretion is most difficult in massive disks and at large orbital distances.

Subject headings: solar system: formation — planets and satellites: formation — accretion, accretion disks — turbulence

1. Introduction

It is often considered that the evolution of protoplanetary disks and the consequent accretion of gas by the central protostar are driven by turbulent viscosity due to a Magneto-Rotational-Instability (MRI) (e.g., Balbus & Hawley 1991). Laughlin et al. (2004) and Nelson & Papaloizou (2004) carried out fluid dynamical simulations of MRI and found that the random torques due to the turbulent density fluctuations give rise to a random walk in semimajor axes of planetesimals. Rice & Armitage (2003) pointed out through model calculations that the random walk expands the effective feeding zone of protoplanets, and may lead to rapid formation of large cores for gas giants. Through a Fokker-Planck treatment, Johnson et al. (2006) also pointed out the importance of the random walk in planet accretion. Adopting the semi-analytical formula for the random torque derived by Laughlin et al. (2004), Ogihara et al. (2007) performed N-body simulations for the late stages of terrestrial planet accretion with a disk significantly depleted in gas, starting from Mars-mass protoplanets. They found that the MRI turbulence indeed helps to reduce the number of accreted terrestrial planets which is otherwise too large compared to our Solar System.

However, Nelson (2005) found through direct integrations of the orbits of protoplanets in a MRI turbulent disk that orbital eccentricities are also excited. Britsch et al. (2008) also found a similar feature in a self-gravitating disk. While the random walk itself is favorable to the growth of protoplanets by avoiding isolation, the excitation of their eccentricities, which had been neglected in Rice & Armitage (2003) and Johnson et al. (2006), is a threat for planetesimal accretion processes because of increased collision velocity. Unfortunately, Nelson (2005)'s orbital integrations were limited to 100–150 Keplerian times and neglected collision processes, so that it is not possible to conclude from that work whether planetesimals should grow or be eroded in the presence of turbulence.

In the present article, we explore by which paths planetesimals may have grown to planet-sized bodies in turbulent disks. Because the level of density fluctuations due to the MRI turbulence is not well determined, we choose to study the qualitative effects of the turbulence on the accretion of planetesimals and their dependence on the key parameters of the problem, in particular the progressive removal of the gas disk. In §2, we summarize the conditions for the accretion and destruction of planetesimals in terms of their orbital eccentricities. In §3, we analytically derive the equilibrium eccentricity for which the excitation due to turbulence is balanced by damping due to tidal interactions with the disk gas, aerodynamic gas drag, and collisions. Comparing the equilibrium eccentricities with critical eccentricities for accretion and destruction, we derive critical physical radii and masses of planetesimals for accretion or destruction. The results are applied to viscously evolving disks (§4). We then discuss possible solutions for the problem of the formation of planetesimals

and planets (§5).

2. Accretion and destruction conditions

We summarize the accretion and destruction conditions below. From energy conservation, the collision velocity ($v_{\rm coll}$) between two planetesimals (labeled 1 and 2) satisfies

$$E = \frac{1}{2}v_{\rm coll}^2 - \frac{G(M_1+M_2)}{R_1+R_2} = \frac{1}{2}v_{\rm rel}^2, \quad (1)$$

where M_j and R_j are the mass and physical radius of a planetesimal j ($j=1,2$), and $v_{\rm rel}$ is their relative velocity when they are apart from each other. When the velocity dispersion of planetesimals $v_{\rm disp}$ is larger than the Hill velocity that is given by $(M/3M_*)^{1/3}v_{\rm K}$, where M_* is the mass of the host star and $v_{\rm K}$ is the Keplerian velocity, $v_{\rm rel}$ is approximated by $v_{\rm disp}$ (e.g., Ida & Nakazawa 1989; Ida 1990). The total energy then becomes:

$$2E = v_{\rm coll}^2 - v_{\rm esc}^2 \simeq v_{\rm disp}^2, \quad (2)$$

where $v_{\rm esc}$ is the (two-body) surface escape velocity defined by

$$v_{\rm esc} = \sqrt{\frac{2G(M_1+M_2)}{R_1+R_2}}. \quad (3)$$

Collisional dissipation decreases the energy by some fraction of $v_{\rm coll}^2/2$. If $v_{\rm disp} \ll v_{\rm esc}$, the collisional dissipation results in $E<0$ after collision. On the other hand, E is likely to be still positive after a collision with $v_{\rm disp} \gg v_{\rm esc}$. Thus, for moderate dissipation, the condition for an accretional collision is $v_{\rm disp} < v_{\rm esc}$ (e.g., Ohtsuki 1993). Since the orbital eccentricity $e \simeq v_{\rm disp}/v_{\rm K}$, a collision should result in accretion for $e < e_{\rm acc}$, where

$$\begin{aligned} e_{\rm acc} \simeq \frac{v_{\rm esc}}{v_{\rm K}} &\simeq 0.28\left(\frac{M}{M_\oplus}\right)^{1/3}\left(\frac{\rho_{\rm p}}{3{\rm gcm}^{-3}}\right)^{1/6}\left(\frac{r}{1{\rm AU}}\right)^{1/2} \\ &\simeq 0.036\left(\frac{R}{10^3{\rm km}}\right)\left(\frac{\rho_{\rm p}}{3{\rm gcm}^{-3}}\right)^{1/2}\left(\frac{r}{1{\rm AU}}\right)^{1/2}. \end{aligned} \quad (4)$$

In the above relation, $\rho_{\rm p}$ is the bulk density of the planetesimals and $M \sim M_j$ (for simplicity, $M_1 \sim M_2$ is assumed). The physical radius R is given by

$$R = 7.8\times 10^8 (M/M_\oplus)^{1/3}(\rho_{\rm p}/3{\rm gcm}^{-3})^{-1/3}{\rm cm}. \quad (5)$$

A collision results in destruction if the collision velocity is such that the specific kinetic energy of a collision ($v_{\rm col}^2/2$) exceeds

$$Q_{\rm D} \simeq \left[Q_0\left(\frac{R}{1{\rm cm}}\right)^a + 3B\left(\frac{\rho_{\rm p}}{3{\rm gcm}^{-3}}\right)\left(\frac{R}{1{\rm cm}}\right)^b\right]{\rm erg/g}, \quad (6)$$

where Q_0 is the material strength, $B \simeq 0.3$–2.1, $a \simeq -0.4$, and $b \simeq 1.3$ (Benz & Asphaug 1999). For basalt rocks or water ice, $Q_0 \simeq 10^7$–10^8 (Benz & Asphaug 1999), but it can take a significantly smaller value for loose aggregates. [1]

We adopt $Q_0 = 3 \times 10^7$ as a nominal value. Self-gravity (the second term in the r.h.s.) dominates the material strength when $R \gtrsim 100$ m. In this regime, adopting $B \sim 1$, a collision results in destruction for $e > e_{\rm dis}$, where

$$\begin{aligned} e_{\rm dis} \simeq \frac{\sqrt{2Q_{\rm D}}}{v_{\rm K}} &\simeq 0.50 \left(\frac{M}{M_\oplus}\right)^{0.22} \left(\frac{\rho_{\rm p}}{3{\rm gcm}^{-3}}\right)^{0.28} \left(\frac{r}{1{\rm AU}}\right)^{1/2} \\ &\simeq 0.13 \left(\frac{R}{10^3{\rm km}}\right)^{0.65} \left(\frac{\rho_{\rm p}}{3{\rm gcm}^{-3}}\right)^{0.5} \left(\frac{r}{1{\rm AU}}\right)^{1/2}. \end{aligned} \tag{7}$$

3. Equilibrium eccentricities

We first derive the equilibrium eccentricities of planetesimals at which the excitation by the MRI turbulence is balanced by damping due to drag and/or collisions. Comparing the estimated eccentricities with $e_{\rm acc}$ and $e_{\rm dis}$, we then evaluate the outcome of collisions between planetesimals as a function of planetesimal size, turbulent strength, and surface density of disk gas.

For an easy interpretation, we provide in this section analytical relations based on a model in which the gas and solid components of disk surface density are scaled with the multiplicative factors f_g and f_d:

$$\Sigma_g = 2400 f_g \left(\frac{r}{1{\rm AU}}\right)^{-3/2} \ {\rm g\,cm}^{-2}, \tag{8}$$

and

$$\Sigma_d = 10 f_d \eta_{\rm ice} \left(\frac{r}{1{\rm AU}}\right)^{-3/2} \ {\rm g\,cm}^{-2}, \tag{9}$$

where $\eta_{\rm ice} \simeq 3$–4 is an enhancement factor of Σ_d due to ice condensation. If $f_g = f_d = 1$, Σ_g and Σ_d are 1.4 times those of the minimum mass solar nebula model (Hayashi 1981).

In this section, we also use the disk temperature distribution obtained in the optically thin limit (Hayashi 1981),

$$T \simeq 280 \left(\frac{r}{1\,{\rm AU}}\right)^{-1/2} \left(\frac{L_*}{L_\odot}\right)^{1/4} \ {\rm K}, \tag{10}$$

[1] For porous materials, Q_0 is rather higher (W. Benz, private communication).

where L_* and $L_\odot$ are the stellar and solar luminosities, respectively. The corresponding sound velocity is

$$c_s = 1.1 \times 10^5 \left(\frac{r}{1\,\mathrm{AU}}\right)^{-1/4} \left(\frac{L_*}{L_\odot}\right)^{1/8} \ \mathrm{cm/s}. \tag{11}$$

Since the disk scale height is given by $h = \sqrt{2}c_s/\Omega_\mathrm{K}$ (assuming that T is vertically uniform in the disk), eqs. (8) and (11) yield the disk gas density at the midplane as

$$\rho_g = \frac{\Sigma_g}{\sqrt{\pi}h} = 2 \times 10^{-9} f_g \left(\frac{r}{1\,\mathrm{AU}}\right)^{-11/4} \ \mathrm{gcm}^{-3}. \tag{12}$$

3.1. Excitation

The orbital eccentricities of planetesimals are pumped up both by the random gravitational perturbations from density fluctuations of disk gas, as well as by mutual gravitational scattering among planetesimals. Assuming planetesimals have equal masses, their orbital eccentricities should be excited to at most $\sim e_\mathrm{acc}$ by the mutual scattering (e.g., Safronov 1969). As will be shown below, the value of this excentricity is smaller than that due to the turbulent excitation, except for very large planetesimals ($\sim 10^3$ km or larger), and/or in the case of significantly depleted gas disks. For simplicity, in this work we choose to neglect the possibility that mutual scattering dominates over turbulent excitation. It is therefore important to note that our results may be slightly optimistic when concerning the possibility of accretion of massive planetesimals.

The orbital eccentricities that result from the turbulent density fluctuations in the disk are provided by Ogihara et al. (2007) on the basis of orbital integrations with empirical formula by Laughlin et al. (2004), as

$$e \sim 0.1\gamma \left(\frac{\Sigma_g}{\Sigma_{g,1}}\right) \left(\frac{r}{1\mathrm{AU}}\right)^2 \left(\frac{t}{T_\mathrm{K}}\right)^{1/2} = 0.1 f_g \gamma \left(\frac{r}{1\mathrm{AU}}\right)^{-1/4} \left(\frac{t}{1\mathrm{year}}\right)^{1/2}, \tag{13}$$

where $\Sigma_{g,1}$ is Σ_g at 1AU with $f_g = 1$ (eq. [8]) and γ is a non-dimensional parameter to express the disk turbulence. [2] Although Ogihara et al. (2007) showed the results only at

---

[2] Although Ogihara et al. (2007) suggested that eq. (13) may be enhanced by a factor 10 by the inclusion of $m = 1$ modes, the $m = 1$ modes actually enhance only the amplitude of random walk in semimajor axis (Δa) but not the eccentricity. Since higher m modes fluctuate over shorter timescales, they tend to cancel out on the orbital period of a planetesimal. For these modes, $\Delta a/a$, which is due to time variation of the potential, is much smaller than Δe, because the latter is also excited by the non-axisymmetric structure. The inclusion of slowly varying $m = 1$ modes enhances $\Delta a/a$ up to the order of $\sim e$. On the other hand, the definition of Γ in eqs. (5) and (34) of Ogihara et al. (2007) should be multiplied by π. We use eq. (13) for the eccentricity excitation, which is consistent with an orbital calculation including $m = 1$ modes (figure 1).

$\sim$ 1AU, we here added a dependence on r using scaling arguments (see the Appendix). Orbital integration for other r show a consistent dependence. Note that $\Delta a/a \sim e$, where Δa is the amplitude of random walk in semimajor axis. Since $e \ll 1$, the radial distance r and semimajor axis a are identified here.

From the simulation results by Laughlin et al. (2004), the value of γ may be $\sim (1/3)(\delta\rho/\rho) \sim 10^{-3}$–$10^{-2}$ for MRI turbulence. In this paper, we use $\gamma = 10^{-3}$ as a fiducial value. Interestingly, with a quite different approach, Johnson et al. (2006) derived a similar formula for $\Delta a/a$ with the same dependences on r, Σ_g and t. If $e \simeq \Delta a/a$, their formula is consistent with ours. They suggested that $\gamma \sim \alpha$ or $\alpha^{1/2}h/a$ where h is disk scale height and α is the parameter for the alpha prescription for turbulent viscosity (Shakura & Sunyaev 1973). For $\alpha = 10^{-3}$–10^{-2}, their estimate is also similar to our fiducial value.

The top panels in fig. 1 show the results of an orbital integration with 4-th order Hermite scheme for the evolution of e and $\Delta a/a$ with turbulent perturbations but without any damping. Five independent runs with different random number seeds for the generation of turbulent density fluctuations (Ogihara et al. 2007) are plotted in each panel. The initial e and i are 10^{-6}. For $f_g = 1$, $\gamma = 0.01$, and $r = 1$AU, as used in fig. 1, eq. (13) is reduced to $e \sim 10^{-3}(t/1\mathrm{year})^{1/2}$. To highlight the effect of turbulence, we used a larger value of γ than the fiducial value. The evolution of the root mean squares of the five runs in fig. 1 agrees with eq. (13) within a factor of ~ 2. From eq. (13), the excitation timescale is

$$\tau_{\mathrm{exc}} = \frac{e}{de/dt} \simeq 2 \times 10^2 \gamma^{-2} e^2 \left(\frac{\Sigma_g}{\Sigma_{g,1}}\right)^{-2} \left(\frac{r}{1\mathrm{AU}}\right)^{-4} T_{\mathrm{K}} = 2 \times 10^2 f_g^{-2} \gamma^{-2} e^2 \left(\frac{r}{1\mathrm{AU}}\right)^{1/2} \text{ years.} \tag{14}$$

3.2. Damping

The eccentricity damping processes are i) tidal interaction with disk gas, ii) aerodynamical gas drag, and iii) inelastic collisions. The tidal damping timescale (i) is derived by Tanaka & Ward (2004) as

$$\tau_{\mathrm{tidal}} \simeq 1.3 \left(\frac{M}{M_\odot}\right)^{-1} \left(\frac{\Sigma_g r^2}{M_\odot}\right)^{-1} \left(\frac{c_s}{v_{\mathrm{K}}}\right)^4 \Omega_{\mathrm{K}}^{-1} \simeq 3 \times 10^2 f_g^{-1} \left(\frac{M}{M_\oplus}\right)^{-1} \left(\frac{r}{1\mathrm{AU}}\right)^2 \text{ years.} \tag{15}$$

The gas drag damping timescale (ii) is derived by Adachi et al. (1976) as

$$\tau_{\mathrm{drag}} \simeq \frac{M v_{\mathrm{disp}}}{\pi R^2 \rho_g v_{\mathrm{disp}}^2} \simeq 2 \times 10^4 f_g^{-1} e^{-1} \left(\frac{M}{M_\oplus}\right)^{1/3} \left(\frac{\rho_{\mathrm{p}}}{3\mathrm{gcm}^{-3}}\right)^{2/3} \left(\frac{r}{1\mathrm{AU}}\right)^{13/4} \text{ years.} \tag{16}$$

For simplicity, we evaluate the damping timescale due to inelastic collision as the mean collision time of planetesimals, assuming that all the planetesimals have the same mass M. Since in the size distribution caused by collision cascade, collisions with comparable-sized bodies and those with smaller ones contribute similarly, the neglection of the size distribution may not be too problematic. Since we look for the conditions in which collisions are non-accretional, we consider the case with $v_{\rm disp} > v_{\rm esc}$. Assuming that the gravitational focusing factor $[1 + (v_{\rm esc}/v_{\rm disp})^2] \sim 1$, the collision damping timescale is

$$\tau_{\rm coll} \simeq \frac{1}{n\pi R^2 v_{\rm disp}} \simeq 2 \times 10^7 f_d^{-1} \eta_{\rm ice}^{-1} \left(\frac{M}{M_\oplus}\right)^{1/3} \left(\frac{\rho_{\rm p}}{3{\rm gcm}^{-3}}\right)^{2/3} \left(\frac{r}{1{\rm AU}}\right)^3 {\rm years}, \tag{17}$$

where n is the spatial number density of planetesimals. Note that $n \sim (\Sigma_d/M)/(v_{\rm disp}/\Omega_{\rm K})$.

3.3. Equilibrium eccentricity

We now equate eq. (14) with eqs. (15), (16), and (17), respectively, to obtain an equilibrium eccentricity for each damping process. For simplicity and to a good approximation, the actual equilibrium eccentricity can be approximated as the minimum of the three equilibrium eccentricities. From eqs. (14) and (15),

$$\begin{aligned} e_{\rm tidal} &\simeq 1.2 f_g^{1/2} \gamma \left(\tfrac{M}{M_\oplus}\right)^{-1/2} \left(\tfrac{r}{1{\rm AU}}\right)^{3/4} \\ &\simeq 24 f_g^{1/2} \gamma \left(\tfrac{R}{10^3{\rm km}}\right)^{-3/2} \left(\tfrac{\rho_{\rm p}}{3{\rm gcm}^{-3}}\right)^{-1/2} \left(\tfrac{r}{1{\rm AU}}\right)^{3/4}. \end{aligned} \tag{18}$$

With eq. (16),

$$\begin{aligned} e_{\rm drag} &\simeq 4.6 f_g^{1/3} \gamma^{2/3} \left(\tfrac{M}{M_\oplus}\right)^{1/9} \left(\tfrac{\rho_{\rm p}}{3{\rm gcm}^{-3}}\right)^{2/9} \left(\tfrac{r}{1{\rm AU}}\right)^{11/12} \\ &\simeq 0.23 f_g^{1/3} \gamma^{2/3} \left(\tfrac{R}{1{\rm km}}\right)^{1/3} \left(\tfrac{\rho_{\rm p}}{3{\rm gcm}^{-3}}\right)^{1/3} \left(\tfrac{r}{1{\rm AU}}\right)^{11/12}. \end{aligned} \tag{19}$$

For $f_g = 1$, $\gamma = 0.01$, and $r = 1$AU, eq. (19) predicts that $e_{\rm drag} \simeq 0.045$ for $M/M_\oplus = 10^{-6}$ and $e_{\rm drag} \simeq 0.01$ for $M/M_\oplus = 10^{-12}$. An orbital integration in the middle and bottom panels in fig. 1 shows that the results agree with the analytical estimate within a factor ~ 1.5. With eq. (17),

$$\begin{aligned} e_{\rm coll} &\simeq 3.2 \times 10^2 f_g (f_d \eta_{\rm ice})^{-1/2} \gamma \left(\tfrac{M}{M_\oplus}\right)^{1/6} \left(\tfrac{\rho_{\rm p}}{3{\rm gcm}^{-3}}\right)^{1/3} \left(\tfrac{r}{1{\rm AU}}\right)^{5/4} \\ &\simeq 3.6 f_g (f_d \eta_{\rm ice})^{-1/2} \gamma \left(\tfrac{R}{1{\rm km}}\right)^{1/2} \left(\tfrac{\rho_{\rm p}}{3{\rm gcm}^{-3}}\right)^{5/6} \left(\tfrac{r}{1{\rm AU}}\right)^{5/4}. \end{aligned} \tag{20}$$

In figure 2, the equilibrium eccentricity, $e_{\rm eq} = \min(e_{\rm tidal}, e_{\rm drag}, e_{\rm coll})$, is plotted with solid lines as a function of the planetesimal radius R, the corresponding planetesimal mass

being $M = 2.1 \times 10^{-3}(R/10^3\mathrm{km})^3(\rho_\mathrm{p}/3\mathrm{gcm}^{-3})M_\oplus$, Note again that the effect of mutual planetesimal scattering is neglected. For bodies with more than Lunar to Mars masses, tidal damping is dominant. This yields a decrease in the equilibrium eccentricity with increasing planetesimal radius for $R \gtrsim 100$km. For smaller mass bodies, gas drag damping dominates tidal damping and the equilibrium eccentricity increases with increasing R. For the smallest planetesimal sizes (the regions with the slightly steeper positive gradient), collision damping is dominant, but with a significant contribution of gas drag damping.

The limiting mass and radius at which e_drag (eq. [19]) and e_acc (eq. [4]) cross are

$$\begin{aligned} M_\mathrm{acc} &\simeq 3.0 \times 10^{-4} f_g^{3/2} \left(\tfrac{\gamma}{10^{-3}}\right)^3 \left(\tfrac{\rho_\mathrm{p}}{3\mathrm{gcm}^{-3}}\right)^{-1/4} \left(\tfrac{r}{1\mathrm{AU}}\right)^{9/8} M_\oplus, \\ R_\mathrm{acc} &\simeq 5.2 \times 10^2 f_g^{1/2} \left(\tfrac{\gamma}{10^{-3}}\right) \left(\tfrac{\rho_\mathrm{p}}{3\mathrm{gcm}^{-3}}\right)^{-5/12} \left(\tfrac{r}{1\mathrm{AU}}\right)^{3/8} \mathrm{km}. \end{aligned} \tag{21}$$

The accretion of planetesimals is possible for $M > M_\mathrm{acc}$ ($R > R_\mathrm{acc}$). In the top panel of fig. 2 ($\gamma = 10^{-3}$ and $f_g = 1$), planetesimal accretion proceeds in a range of R's in which the solid line (e_eq) is located below the dashed line (e_acc), that is, only if a body is larger than Ceres. Such large planetesimals can be formed by a different mechanism than pairwise accretion such as self-gravitational instability in turbulent eddies (e.g., Johansen et al. 2007). When the disk gas is removed, accretion becomes possible for smaller planetesimals (the 2nd panel of fig. 2). On the other hand, if turbulence is stronger ($\gamma \sim 10^{-2}$), planetesimal accretion requires more than 1000 km-sized bodies. This appears to be an insurmountable barrier to accretion, even for depleted gaseous disks ($f_g \sim 0.1$), as shown in the the 3rd panel of fig. 2. Finally, at large orbital radii, planetesimal accretion is even more difficult (the bottom panel).

Another critical mass (radius) is the point at which e_drag (eq. [19]) and e_dis in the gravity regime (eq. [7]) cross,

$$\begin{aligned} M_\mathrm{dis} &\simeq 6 \times 10^{-11} f_g^{3.3} \left(\tfrac{\gamma}{10^{-3}}\right)^{6.7} \left(\tfrac{\rho_\mathrm{p}}{3\mathrm{gcm}^{-3}}\right)^{-0.6} \left(\tfrac{r}{1\mathrm{AU}}\right)^{4.2} M_\oplus, \\ R_\mathrm{dis} &\simeq 3 f_g^{1.1} \left(\tfrac{\gamma}{10^{-3}}\right)^{2.2} \left(\tfrac{\rho_\mathrm{p}}{3\mathrm{gcm}^{-3}}\right)^{-0.53} \left(\tfrac{r}{1\mathrm{AU}}\right)^{1.4} \mathrm{km}. \end{aligned} \tag{22}$$

Planetesimals with $M < M_\mathrm{dis}$ ($R < R_\mathrm{dis}$) are disrupted by collisions down to the sizes for which material strength is dominant (see below). For $\gamma \sim 10^{-3}$ and $f_g \sim 1$ (the top panel of fig. 2), planetesimals with sizes larger than several km radius survive but without growing, while smaller planetesimals are disrupted.

When a planetesimal is smaller than ~ 100 m in size, it is bounded by material strength rather than self-gravity. In the regime of material strength, $Q_\mathrm{D} \sim Q_0(R/1\mathrm{cm})^{-0.4}$. The body

is not disrupted if $\sqrt{2Q_{\rm D}}/v_{\rm K} > e_{\rm drag}$, which is equivalent to

$$\begin{aligned} M &\lesssim M_{\rm mat} \simeq 0.8 \times 10^{-17} f_g^{-1.9} \left(\frac{\gamma}{10^{-3}}\right)^{-3.7} \left(\frac{\rho_{\rm p}}{3{\rm gcm^{-3}}}\right)^{-0.9} \left(\frac{r}{1{\rm AU}}\right)^{2.8} M_\oplus, \\ R &\lesssim R_{\rm mat} \simeq 16 f_g^{-0.62} \left(\frac{\gamma}{10^{-3}}\right)^{-1.25} \left(\frac{\rho_{\rm p}}{3{\rm gcm^{-3}}}\right)^{-0.62} \left(\frac{r}{1{\rm AU}}\right)^{2.8} {\rm m}. \end{aligned} \tag{23}$$

Since in this regime, collision damping is slightly stronger than gas drag, actual values of $M_{\rm mat}$ and $R_{\rm mat}$ are determined by $\sqrt{2Q_{\rm D}}/v_{\rm K} > e_{\rm coll}$, so they are slightly larger than the above estimate (see fig. 2). When $\tau_{\rm drag}\Omega_{\rm K} \lesssim 1$, the planetesimals' motions are coupled to that of the gas. The collision velocity then cannot be expressed in terms of orbital eccentricity. This limiting size is however much smaller than $R_{\rm mat}$. The collision cascade would hence stop at $M \sim M_{\rm mat}$ ($R \sim R_{\rm mat}$). Regions for which the dotted lines ($e_{\rm dis}$) in fig. 2 have negative gradients correspond to the material strength regime. In the depleted disk case, $e_{\rm dis}$ is always larger than $e_{\rm eq}$, so that the disruptive regions do not exist (see the 2nd panel of fig. 2). Note that $R_{\rm mat} \propto Q_0^{0.94}$. If the planetesimals are loose aggregates so that $Q_0 < 3 \times 10^7$ (the value for basalt rocks or water ice), the limiting size $R_{\rm mat}$ is smaller.

4. Accretion/destruction of planetesimals in an evolving disk

We now put these various critical physical radii in the context of the evolution of the protoplanetary disk. In order to investigate the effect of departures from power-law relations of the surface density and temperature profiles in real disks, we also present in this section results obtained from a 1D disk model that includes an α-viscosity and photoevaporation (see Guillot & Hueso 2006; Hueso & Guillot 2005). The parameters used in the model presented here are a turbulent viscosity $\alpha = 0.01$ and an evaporation parameter $T_{\rm atm} = 100\,{\rm K}$ (the temperature of the evaporation part of the outer disk). Another choice of the parameters would affect the results only marginally.

In the numerical calculation in this section, we evaluate the equilibrium eccentricities $e_{\rm eq}$ as a function of planetesimal radius by solving the following relation:

$$\tau_{\rm exc}^{-1} = \tau_{\rm tidal}^{-1} + \tau_{\rm drag}^{-1} + \tau_{\rm coll}^{-1}, \tag{24}$$

where the different timescales are given by eqs. (14) to (17). The survival physical radius for accretion $R_{\rm acc}$ is then found, for each orbital radius in the protoplanetary disk and for each timestep, by solving the equation,

$$e_{\rm eq}(R_{\rm acc}) = e_{\rm acc}(R_{\rm acc}), \tag{25}$$

where $e_{\rm acc}$ is given by eq. (4). When the mean kinetic energy is larger than the strength of a planetesimal, the a collision is highly erosive. We then obtain the range $R < R_{\rm dis}$

corresponding to the highly erosive collisions by solving the equation,

$$e_{\rm eq}(R_{\rm dis}) = \frac{\sqrt{2Q_{\rm D}(R_{\rm dis})}}{v_{\rm K}}, \tag{26}$$

where $Q_{\rm D}$ is given by eq. (6).

Figures 3 to 5 show our results for three values of the turbulent excitation parameter, $\gamma = 10^{-2}$, 10^{-3} (our fiducial value), and 10^{-4}. Each figure shows, for three orbital distances, 1, 5 and 30 AU, the planetesimal physical radii corresponding to accretive and erosive regions are plotted as a function of the total mass remaining in the disk. Since the disk mass decreases with time as a result of viscous evolution and photoevaporation, a decrease in disk mass corresponds to evolution in time. As shown in the previous section, planetesimal accretion becomes easier as the disk becomes less massive simply because the turbulent excitation, directly proportional to the local surface density of the gas, becomes weaker. However, after some point, the disk becomes too light to provide a sufficient amount of gas to form Jupiter-mass gas giants.

The figures also show as thin black lines the values obtained for a disk that follows the slope in surface density versus orbital distance defined for the MMSN (eq. 8) as a function of a disk mass. The disk mass in this model is given by $3.4 \times 10^{-2} f_g (r_{\rm edge}/100{\rm AU})^{1/2} M_\odot$, where $r_{\rm edge}$ is the outer edge radius of the disk. Although the original MMSN model by Hayashi (1981) used $r_{\rm edge} = 35$ AU, we here adopt $r_{\rm edge} = 1000$ AU (for comparison, our fiducial alpha disk model with $T_{\rm atm} = 100\,{\rm K}$ extends up to a maximum of 350 AU).

These are found to be in excellent agreement with the analytical expressions derived in the previous section, with small differences arising from the simplifications inherent to the analytical approach. Larger differences are found between the power-law disk and the α-disk models mostly because of the difference in slopes ($d\ln\Sigma/d\ln r = -3/2$ for the former, ~ -1 for the α-disk) which implies that a given disk mass does not correspond to the same surface density with two models, the difference being larger at smaller orbital distances. However, the qualitative features of accretive and erosive regions are similar to each other. It should be noted that the models also differ in their temperature profiles, but this is found to be less important.

In the highly turbulent regime presented in fig. 3, a self-sustained regime of accretion becomes possible only when planetesimals have become very large/massive, with sizes generally well over 100km. This case also yields a sustained area of high erosion where the average kinetic energies of planetesimals are above their internal energies. It is difficult to imagine how planetary cores can form in this context especially if they have to grow large enough to form giant planets.

With smaller perturbations from the turbulent disk (fig. 4), planetesimals have more possibilities to accrete: with time, as the disk mass decreases, the inner disk rapidly moves out of the highly erosive regime, while erosion still remains important at large orbital distances. With a turbulence strength parameter $\gamma = 10^{-4}$, corresponding to a very weak turbulence (fig. 5), the presence of a highly erosive regime centered around $\sim$ 300m planetesimals is limited only to the outer regions ($\gtrsim$ 30 AU), and the zone rapidly shrinks as the circumstellar gaseous disk disappears.

In order to put these findings into context, we also show the mass of the disk when Jupiter is believed to have started accreting its gaseous envelope. These values are calculated by assuming that the planet growth has been limited mostly by viscous diffusion in the disk, with the protoplanet capturing between 10% and 70% of the mass flux at its orbital distance in the disk evolution model by Hueso & Guillot (2005) (for details, see Guillot & Hueso 2006). If giant planets have to form, at some time corresponding to the disk mass interval defined by the hashed areas in figs. 3 to 5, protoplanetary cores must be already large enough to start accreting the surrounding hydrogen and helium gas.

We can now define three important disk masses, and their corresponding disk ages (with the caution that ages are inherently model-dependent and are provided here for illustrative purposes only, on the basis of our particular model of α-disk evolution with photoevaporation):

1. The maximum mass of the disk, following the collapse of the molecular cloud. This mass can vary quite significantly from one disk formation/evolution model to another. For the particular model shown here, it is of the order of $0.25\,\mathrm{M}_\odot$, for an age of 0.6 Myrs.

2. The disk mass necessary for Jupiter to grow to its present mass if it captures 10% of the mass flux at its orbital distance. For realistic disk models, this depends weakly on parameters such as α and the disk evaporation rate. In our case, it corresponds to $M_{\rm disk} = 0.035\,\mathrm{M}_\odot$ and an age of 1.95 Myrs.

3. The disk mass necessary for Jupiter to grow to its present mass if it captures 70% of the mass flux at its orbital distance. For our model, $M_{\rm disk} = 0.0054\,\mathrm{M}_\odot$ (about 5 times the mass of Jupiter) and an age of 2.85 Myrs.

Table 1 provides the values of the physical radii that define the accretive regime and the highly erosive (disruptive) regime of figs. 3 to 5, namely $R_{\rm acc}$ and $R_{\rm dis}$. In our Solar System, the existence of Jupiter implies that either turbulence was low, the planet grew from a protoplanetary core formed in the inner solar system, or a mechanism was able to lead to the rapid formation of embryos larger than 240 km in radius at 5 AU (17 km in the

low-turbulence case, 1080 km in the high-turbulence case) by the time when the disk mass had decreased to $5 \times 10^{-3}\,\mathrm{M}_\odot$. In the last case, it appears that a mechanism such as the standard gravitational instability (e.g., Safronov 1969; Goldreich & Ward 1973) would not work because of the turbulence, but formation of relatively large protoplanets in eddies or vortexes (e.g., Johansen et al. 2007; Barge & Someria 1995) is a promising possibility.

5. Conclusion and discussion

We have investigated the critical physical radii for collisions between planetesimals to be accretional ($R > R_{\rm acc}$) or disruptive ($R < R_{\rm dis}$) in turbulent disks, as functions of turbulent strength ($\gamma \sim O(\Delta\rho/\rho)$), disk gas surface density, and orbital radius. The results presented here highlight the fact that MRI turbulence poses a great problem for the growth of planetesimals: generally, only those with sizes larger than a few hundred km are in a clearly accretive regime for a nominal value of $\gamma \sim 10^{-3}$. The others generally collide with velocities greater than their own surface escape velocities. For some of them, more severely in the kilometer-size regime, collisions are likely to be disruptive. The problem is greater when the disk is still massive and at large orbital distances. Also, if turbulence is stronger than $\gamma \sim 10^{-2}$, planetesimal accretion becomes extremely difficult.

However, the rate of occurrence of extrasolar giant planets around solar-type stars is inferred to be as large as $\sim 20\%$ (Cumming et al. 2008), and depends steeply on the metallicity of the host star (Fischer & Valenti 2005; Santos et al. 2004). This strongly suggests that the majority of extrasolar giant planets were formed by core accretion followed by gas accretion onto the cores (Ida & Lin 2005). Thus, planetesimals should commonly grow to planetary masses before the disappearance of gas in protoplanetary disks.

The possibilities to overcome the barrier are in principle as follows (their likelihood is commented below):

1. Large M: Large planetesimals with sizes of 100 to 1000 km are formed directly in turbulent environment by a mechanism other than collisional coagulation, jumping over the erosive regime for physical radii.

2. Small Σ_g: Planetesimals start their accretion to planet-size only after the disk surface density of gas has declined to sufficiently small values.

3. Small γ: Planetesimals form in MRI-inactive regions ("dead zones") of protoplanetary disks.

Concerning point 1, the first-born planetesimals with sizes larger than $R_{\rm acc}$ may be formed rapidly by an efficient capture of ∼meter-size boulders in vortexes (Johansen et al. 2007). Such large planetesimals may be consistent with the size distribution of asteroids (Morbidelli et al. 2008). Even if the first-born planetesimals are not as large, a small fraction of them could continue to grow larger than $R_{\rm acc}$ by accreting smaller bodies, because accretion is not completely cut off as soon as $v_{\rm disp} \gtrsim v_{\rm esc}$ (there is always a small possibility for accretion) and the large planetesimals would not be disrupted by smaller ones. This possibility, however, must be examined by a more detailed growth model taking into account the effect of fragmentation and the size distribution of planetesimals, which we neglected in this paper.

Concerning point 2, we have shown that planetesimals are most fragile at early times, in massive disks, and at large orbital distances. We therefore suggest that the growth towards planet sizes may be delayed due to MRI turbulence, and then proceed from inside out: planetesimals should start accretion first close to the star, then progressively at larger orbital distances, as the gas surface density declines. The possibility to delay planet formation while keeping non-migrating km-size planetesimals is noteworthy because it would help planetary systems resisting to type-I migration: they would grow in a gas disk that is less dense, and for which migration timescales may be considerably increased. Ida & Lin (2008a), Alibert et al. (2005), and Daisaka et al. (2006) showed that type-I migration must be lowered by one to two orders of magnitude from the linear calculation (Tanaka et al. 2002) to provide an explanation for the existence of a population of giant planets in agreement with observations. This "late formation" scenario is consistent with the noble gas enrichment in Jupiter (Guillot & Hueso 2006). However, in order to form gas giants, core accretion and gas accretion onto the cores must proceed fast enough to capture Jupiter-mass amount of gas from the decaying gas disk. Once the size of the largest planetesimals exceeds ~ 1000km, their eccentricities are damped by tidal drag and dynamical friction from small bodies. Most of the other small bodies may be ground into sizes smaller than 1 km and their eccentricities could be kept very small by gas drag and collision damping. This could facilitate the runaway accretion of cores to become large enough ($\gtrsim 10 M_\oplus$) for the onset of runaway gas accretion. This issue also has to be addressed by a detailed planetesimal growth model taking into account a size distribution. The likelihood of relatively rapid gas accretion without long "phase 2" is discussed by Shiraishi & Ida (2008). If planetesimal sizes are relatively small, gas drag damping opens up a gap in the planetesimal disk around the orbit of a core and truncates planetesimal accretion onto the core. The truncation of heating due to planetesimal bombardment enables the core to efficiently accrete disk gas.

Concerning point 3, the MRI inactive region ("dead zones") may exist in inner disk regions in which the surface density is large enough to prevent cosmic and X rays from pen-

etrating the disk (Gammie 1996; Sano et al. 2000). The preservation of a dead zone can also contribute to stall type-I migration by converting it to type-II migration (Matsumura et al. 2007) or by creating a local region with a positive radial gradient of disk pressure near the ice line (Ida & Lin 2008b). However, dead zones can be eliminated by turbulent mixing/overshoot (Varnière & Tagger 2006; Turner et al. 2007; Ilgner & Nelson 2008), a self-sustaining mechanism (Inutsuk & Sann 2005), and dust growth (Sano et al. 2000). The last effect comes form the fact that small dust grains are the most efficient agents for charge recombination. According to grain growth, the ionization of the disk and its coupling with the magnetic field become stronger to activate MRI turbulence. We remark that if MRI turbulence is activated, collisions are disruptive and they re-produces small grains to decrease the ionization degree. This self-regulation process might maintain a marginally dead state and keep producing small dust grains. This might be related with relative chronological age difference ($\sim$ 2Myr) between chondrules and CAIs (e.g., Kita et al. 2005). Whether dead zones exist or not is one of the biggest issues in evolution of protoplanetary disks and planet formation. A more detailed analysis of planetesimal accretion in turbulent disks could impose a constraint on this issue.

At large orbital distances (10's of AU), the existence of a highly erosive regime that lasts until late in the evolution of the protoplanetary disk is an important feature of this scenario. It shows that the entire mass of solids is highly reprocessed by collisions, in qualitative agreement with the paucity of presolar grains (intact remnants from the molecular cloud core) found in meteorites. It also prevents the growth of large planetesimals and helps to maintain a large population of small grains in the disks. This is in qualitative agreement with observations that do not indicate a significant depletion of micron-sized grains with time, contrary to what would be predicted in the absence of turbulence (Dullemond & Dominik 2005; Tanaka et al. 2005).

In conclusion, the existence of MRI turbulence may be a threat to planetesimal accretion. Given the uncertainties related to these explanations, we cannot provide a definitive scenario for the formation of protoplanetary cores. However, it offers several promising hints to explain important features of planet formation as constrained by today's observations of protoplanetary disks, exoplanets and meteoritic samples in the Solar System.

This research was supported by the Sakura program between Japan and France, and by the CNRS interdisciplinary program *"Origine des planètes et de la Vie"* through a grant to T.G. and A.M.

Appendix

Here we derive the r-dependence in eq. (13). If the equation of motion is scaled by a reference radius r_1 and $T_{\mathrm{K}1}$ where $T_{\mathrm{K}1}$ is a Keplerian period at r_1, the only remaining non-dimensional parameter in the equations is

$$\gamma\Gamma(r_1) = \gamma\frac{64\Sigma_g r^2}{\pi M_\odot}|_{r_1} \tag{27}$$

(see eqs. [4], [5], [6] in Ogihara et al. (2007)). Consider the equation of motion scaled by r_1 and $T_{\mathrm{K}1}$ and that scaled by r_2 and $T_{\mathrm{K}2}$. If γ is the same and $\Gamma(r_1) = \Gamma(r_2)$, these two scaled-equations of motion are identical and evolution of eccentricity, which is a non-dimensional quantity, must be identical in terms of the scaled time. Note that the magnitude of excited e should be proportional to $\gamma\Gamma$. Since

$$\Gamma(r) = \frac{\Sigma_g(r)}{\Sigma_g(r_1)}\left(\frac{r}{r_1}\right)^2\Gamma(r_1), \tag{28}$$

and Ogihara et al.'s eq. (34) derived for $r = 1\mathrm{AU}$ is proportional to $\gamma\Gamma(1\mathrm{AU})$, the formula for arbitrary r is given by replacing a year by $T_{\mathrm{K}}(r)$ and γ by $\gamma(\Gamma(r)/\Gamma(1\mathrm{AU}))$ in their equation. As a result,

$$e \sim 0.1\gamma\left(\frac{\Sigma_g}{\Sigma_{g,1}}\right)\left(\frac{r}{1\mathrm{AU}}\right)^2\left(\frac{t}{T_{\mathrm{K}}}\right)^{1/2}, \tag{29}$$

where $\Sigma_{g,1}$ is Σ_g at 1AU with $f_g = 1$ (eq. [8]) and the numerical factor was corrected as explained in the footnote in §3.1. Assuming the simple power-law model defined by eq. (7),

$$e \sim 0.1 f_g\gamma\left(\frac{r}{1\mathrm{AU}}\right)^{-1/4}\left(\frac{t}{1\mathrm{year}}\right)^{1/2}. \tag{30}$$

REFERENCES

Adachi, I., Nakazawa, K., & Hayashi, C. 1976, PASJ, 29, 163

Alibert, Y., Mousis, O., Mordasini, C. & Benz, W. 2005, ApJ, 626, 57

Balbus, S. A., & Hawley, J. F. 1991, ApJ, 376, 214

Barge & Someria, 1995, å, 295, 1

Benz, W. & Asphaug, E. 1999, Icarus, 142, 5

Britsch, M., Clarke, C. J. & Lodato, G. 2008, MNRAS, 385, 1067

Cumming, A. Marcy, G.W. Butler, R.P. Fischer, D.A. Vogt, S.S. & Wright, J.T. 2008, in preparation.

Daisaka, K. J., Tanaka, H. & Ida, S. 2006, Icarus, 185, 492

Dullemond, C. P. & Dominik, C. 2005, A&A, 434, 971

Fischer, D. A. & Valenti, J. A. 2005. ApJ, 622, 1102

Gammie, C. F., 1996, Layered accretion in T Tauri disks, ApJ, 457, 355

Goldreich, P. & Ward, W. 1973, ApJ,

Guillot, T. & Hueso, R. 2006, MNRAS, 367, L47

Hayashi, C., 1981, Prog. Theor. Phys. Suppl, 70, 35

Hueso, R. & Guillot, T. 2005, A&A, 442, 703

Ida, S. 1990, Icarus, 88, 129

Ida, S. & Lin, D. N. C. 2005, ApJ, 626, 1045

——. 2008, ApJ, 673, 487

——. 2008, ApJ, in press

Ida, S. & Makino, J. 1993, Icarus, 106, 210

Ida, S. & Nakazawa, K. 1989, å, 224, 303

Ilgner, M., Nelson, R. P., 2008, astro-ph:0802.4409

Inaba, S. & Ikoma, M. å, 410, 711

Inutsuka, S. & Sano, T. å, 410, 711

Johansen, A., Oishi, J. S., Low, M. M., Klahr, H., Thomas, H. & Youdin, A. 2007. Nature, 448, 1022

Kita, N. T. et al. 2005, in Chondrites & the protoplanetary disk, ASP conf. series 341, pp. 558-587

Johnson, E. T., Goodman, J. & Menou, K. 2006, ApJ, 647, 1413

Laughlin, G., Steinacker, A., & Adams, F. C. 2004, ApJ, 608, 489

Matsumura, S., Pudritz, R. E. & Thommes, E. W. 2007, ApJ, 660, 1609

Nelson, R. P., 2005, A&A, 443, 1067

Nelson, R. P., & Papaloizou, J. C. B., 2004, MNRAS, 350, 849

Ohtsuki, K. 1993, Icarus, 106, 228

Ogihara, M., Ida, S. & Morbidelli, A. 2007, Icarus, 188, 522

Rice, W. K. M., Armitage, P J., 2003, ApJ, 598, 55

Safronov, V. 1969, Evolution of thr Protoplanetary Cloud and Formation of the Earth and Planets (Moscow: Nauka Press)

Santos, N., Israelian, G., & Mayor, M., 2004, å, 415, 1153

Sano, T., Miyama, S. M., Umebayashi, T., & Nakano, T., 2000, ApJ, 543, 486

Shakura, N. I. & Sunyaev, R. A. 1973, A&A, 24, 337

Shiraishi, M. & Ida, S. 2008, ApJ, in press.

Tanaka, H., Takeuchi, T. & Ward, W. R., 2002, ApJ, 565, 1257

Tanaka, H., Himeno, Y. & Ida, S. 2005, ApJ, 625, 414

Tanaka, H., & Ward, W. R., 2004, ApJ, 602, 388

Turner, N. J., Sano, T. and Dziourkevitch, N., 2007, ApJ, 659, 729

Varnière, P. & Tagger, M., 2007, ApJ, 446, L13

Table 1: Limits of the accretive regime ($R > R_{\rm acc}$) and the highly erosive (disruptive) regime $R < R_{\rm dis}$, as a function of orbital distance and disk mass.

	1 AU		5 AU		30 AU	
$M_{\rm disk}$ [$M_\odot$]	$R_{\rm acc}$ [km]	$R_{\rm dis}$ [km]	$R_{\rm acc}$ [km]	$R_{\rm dis}$ [km]	$R_{\rm acc}$ [km]	$R_{\rm dis}$ [km]
Fiducial case: $\gamma = 10^{-3}$; $\rho_{\rm p} = 3\,{\rm g\,cm^{-3}}$; $Q_0 = 3\times10^7$; $B = 1.0$						
0.25	280.	[1.14 – 0.061]	1280.	[82. – 0.00047]	1680.	[1000. – 0.00047]
0.035	86.	– –	440.	[5.3 – 0.026]	850.	[200. – 0.0024]
0.0054	46.	– –	240.	[1.05 – 0.057]	590.	[37. – 0.0069]
Low turbulence case: $\gamma = 10^{-4}$; $\rho_{\rm p} = 3\,{\rm g\,cm^{-3}}$; $Q_0 = 3\times10^7$; $B = 1.0$						
0.25	16.	– –	150.	[0.30 – 0.0099]	590.	[22. – 0.0099]
0.035	3.9	– –	36.	– –	220.	[1.07 – 0.053]
0.0054	1.7	– –	17.	– –	103.	– –
High turbulence case: $\gamma = 10^{-2}$; $\rho_{\rm p} = 3\,{\rm g\,cm^{-3}}$; $Q_0 = 3\times10^7$; $B = 1.0$						
0.25	2540.	[300. – 0.0026]	3920.	[2770. – 2×10^{-5}]	4250.	[3220. – 2×10^{-5}]
0.035	870.	[26. – 0.0090]	1590.	[710. – 0.0012]	2180.	[1460. – 0.00012]
0.0054	510.	[7.4 – 0.018]	1080.	[230. – 0.0025]	1580.	[970. – 0.00033]
High material resistance: $\gamma = 10^{-3}$; $\rho_{\rm p} = 3\,{\rm g\,cm^{-3}}$; $Q_0 = 10^8$; $B = 2.0$						
0.25	280.	[0.26 – 0.15]	1280.	[27. – 0.0013]	1680.	[700. – 0.0013]
0.035	86.	– –	440.	[1.6 – 0.068]	850.	[66. – 0.0068]
0.0054	46.	– –	240.	[0.27 – 0.15]	590.	[12. – 0.019]
Low material resistance: $\gamma = 10^{-3}$; $\rho_{\rm p} = 3\,{\rm g\,cm^{-3}}$; $Q_0 = 10^7$; $B = 0.3$						
0.25	280.	[11. – 0.026]	1280.	[550. – 0.00018]	1680.	[1440. – 0.00018]
0.035	86.	[0.56 – 0.087]	440.	[41. – 0.011]	850.	[590. – 0.00097]
0.0054	46.	– –	240.	[9.2 – 0.024]	590.	[240. – 0.0028]

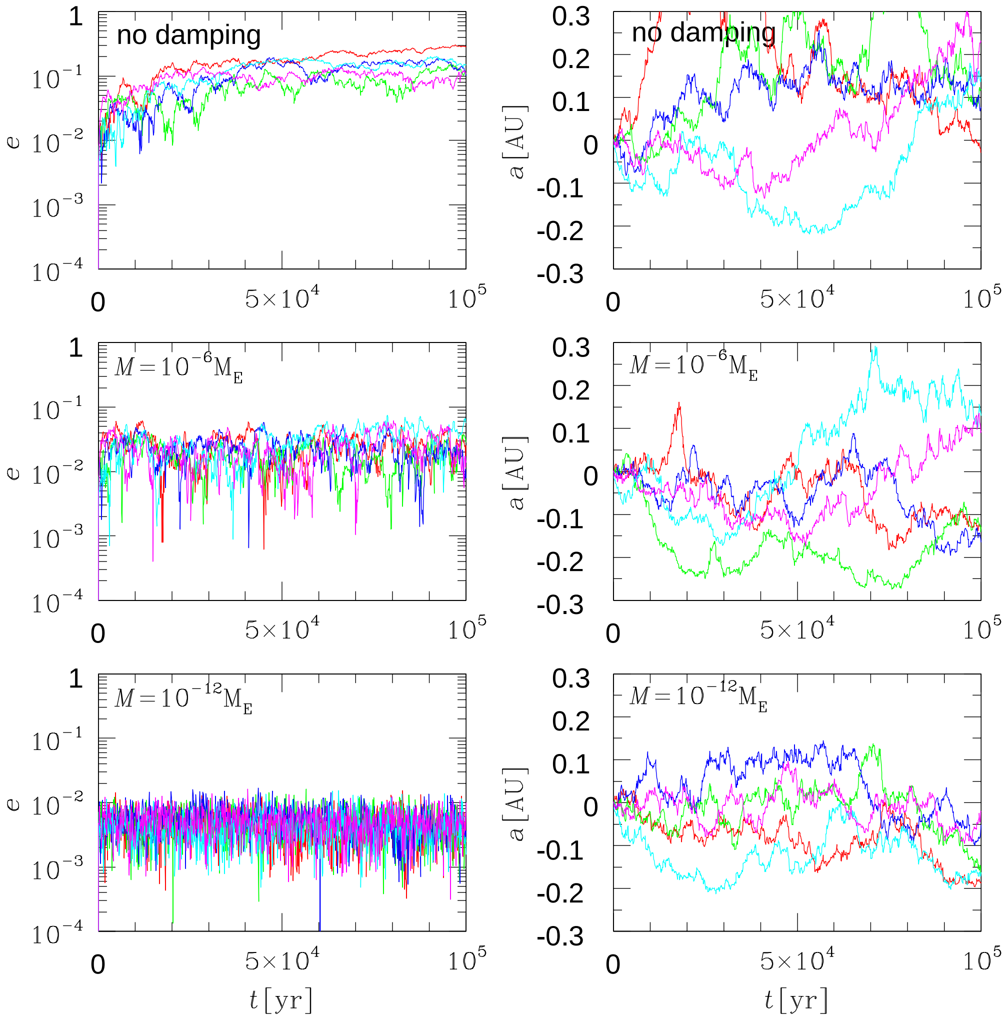

Fig. 1.— Evolution of the eccentricity (left panels) and of the semimajor axis (right panels) as a function of time, for different planetesimal masses (top to bottom). A single planetesimal is integrated in a turbulent disk and 5 independent runs with different random number seeds for the generation of turbulent density fluctuations are shown in each panel. *Top panels*: We consider no tidal and gas drag. *Middle panels*: Results including gas drag for planetesimals of $M = 10^{-6} M_\oplus$. *Bottom panels*: Results for planetesimals of $M = 10^{-12} M_\oplus$. In all cases, we assume an initial orbital distance of 1AU, $f_g = 1$ and $\gamma = 0.01$.

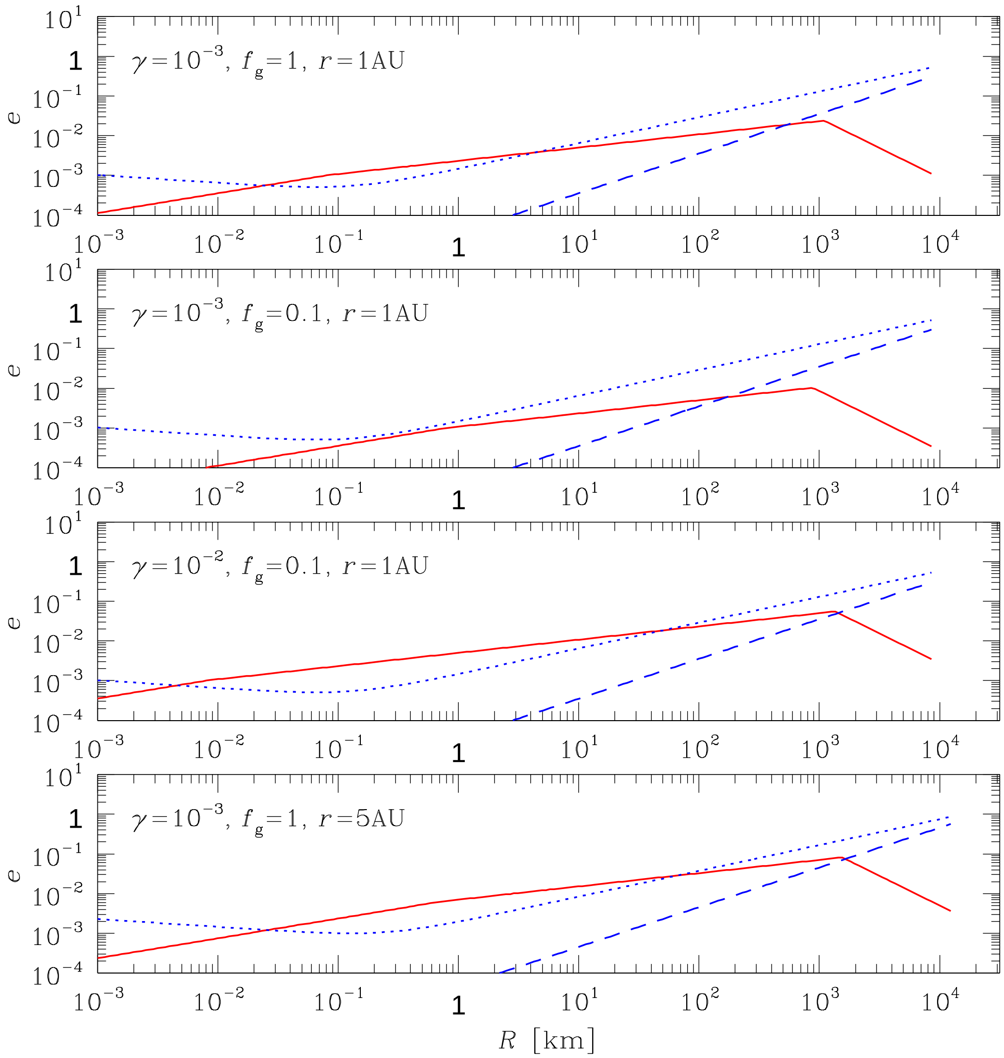

Fig. 2.— Equilibrium eccentricities ($e_{\rm eq}$) as a function of the physical radius R of planetesimals (solid lines). The values of $e_{\rm eq}$ is determined by the minimum of individual equilibrium eccentricities, $e_{\rm tidal}, e_{\rm drag}$, and $e_{\rm coll}$. The critical values for accretion and destruction, $e_{\rm acc}$ and $e_{\rm dis}$, are also plotted by dashed and dotted lines, respectively. At $r = 1$AU, the bulk density $\rho_{\rm p} = 3{\rm gcm}^{-3}$ is assumed, while $\rho_{\rm p} = 1{\rm gcm}^{-3}$ at 5 AU. The mass of the planetesimals is given by $M = 2.1 \times 10^{-3}(R/10^3{\rm km})^3(\rho_{\rm p}/3{\rm gcm}^{-3})M_\oplus$.

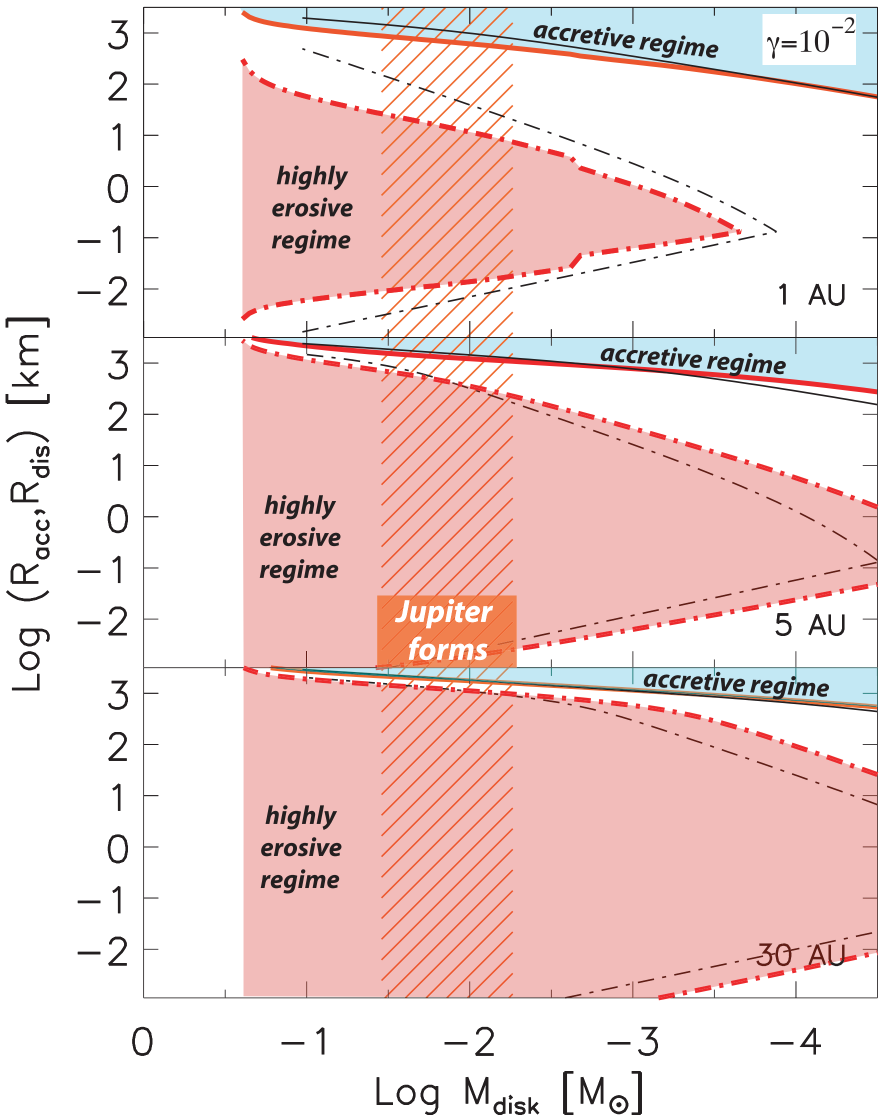

Fig. 3.— Evolution of characteristic physical radii of planetesimals as a function of disk mass, at several orbital distances in the disk: 1AU (top), 5AU (middle) and 30AU (bottom). The solid and dot-dashed curves correspond to the boundary radius for accretion regime ($R_{\rm acc}$) and to that of the highly erosive regime ($R_{\rm dis}$). Two disk models have been used: a simple power-law model with $d\ln\Sigma_g/d\ln r = -3/2$ (eq. [8]) with an outer cut-off radius of 1000AU (thin lines), and an alpha-disk model with $\alpha = 0.01$ and $T_{\rm atm} = 100\,{\rm K}$ (see Guillot & Hueso 2006) (thick lines). The hashed region corresponds to the range of disk mass (equivalently, the range of time if disk evolution is given) during which Jupiter must start accreting hydrogen/helium gas (assuming it grabs between 10% and 70% of the disk mass flux at its orbital distance). In the simulations, MRI turbulence is supposed to be high, with $\gamma = 10^{-2}$. We also choose $Q_0 = 3\times10^7$ and $B = 1$ (see eq. [6]).

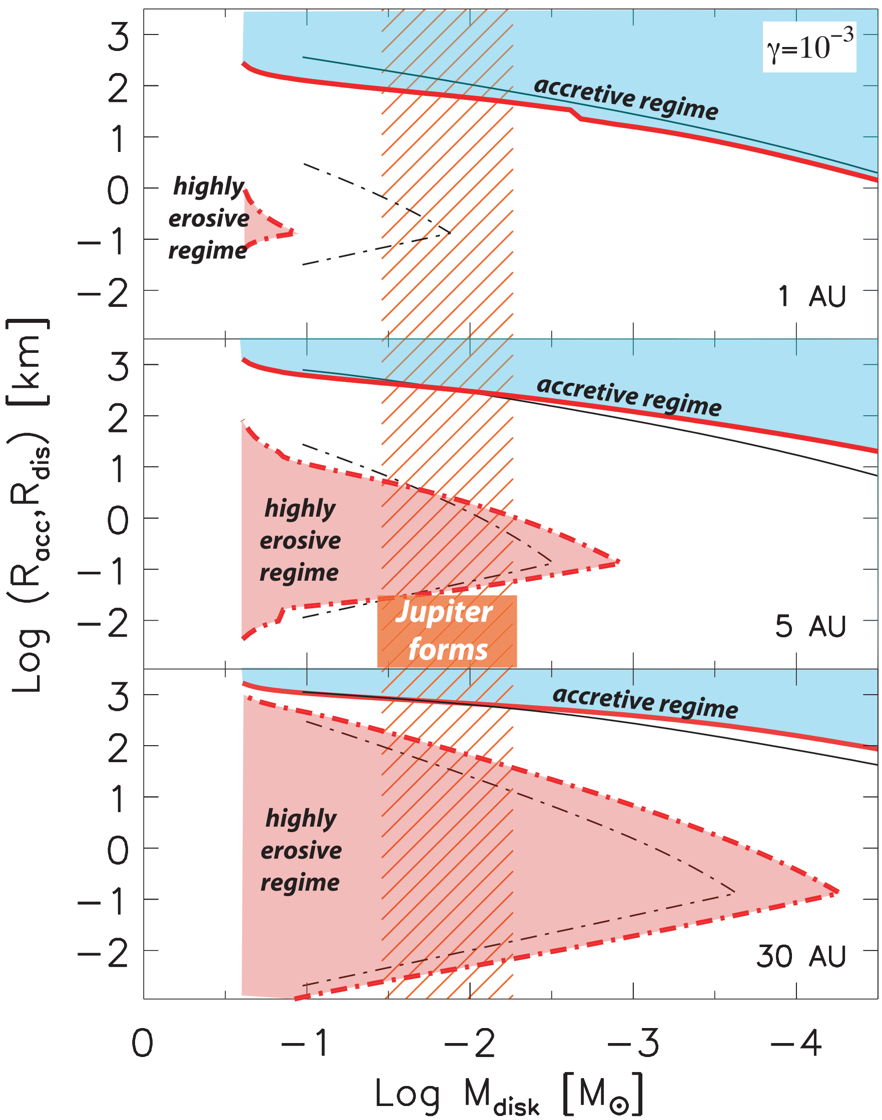

Fig. 4.— Evolution of characteristic physical radii $R_{\rm acc}$ and $R_{\rm dis}$ of planetesimals as a function of disk mass. The parameters and labels are the same as those in fig. 3 but for a medium turbulence case ($\gamma = 10^{-3}$) (our fiducial case).

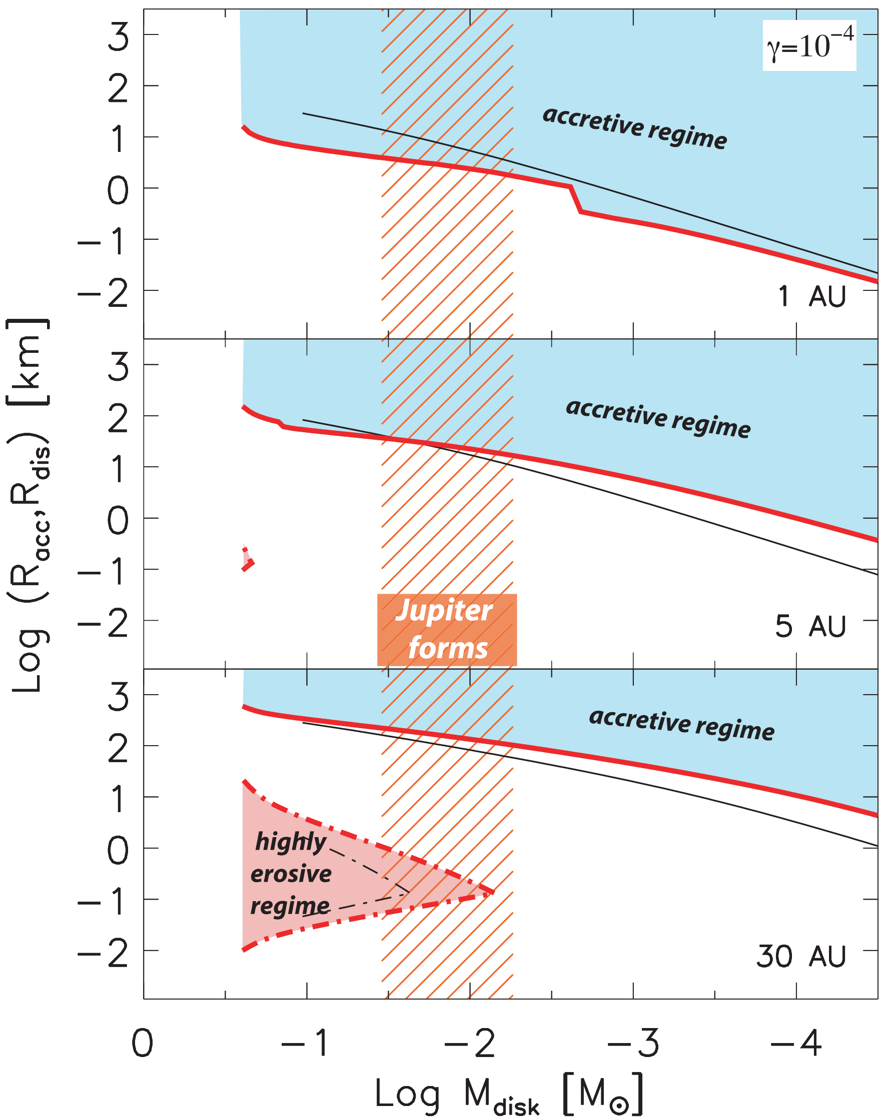

Fig. 5.— Evolution of characteristic physical radii $R_{\rm acc}$ and $R_{\rm dis}$ of planetesimals as a function of disk mass. The parameters and labels are the same as those in fig. 3 but for a weak turbulence case ($\gamma = 10^{-4}$).